Chemical Science & Engineering Research

Ariviyal Publishing

Research Article

DOI: 10.36686/Ariviyal.CSER.2020.02.05.026

Chem. Sci. Eng. Res., 2020, 2(5), 29-39.

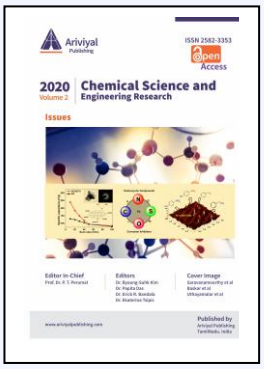

Synthesis of Carica Papaya (Leaf, Peel and Seed) Extracts Mediated Ag Nanoparticles for Industrial and Medical Applications

Supraja N.,*[a] Kishore B.,[b] Rajasekhar K.K.[c] and Padmavathamma M.[d]

[a]*Nanotechnology Laboratory, Institute of Frontier Technology, Regional Agricultural Research Station, Acharya N G Ranga Agricultural University, Tirupati-517 502, AP, India.*

[b]*Department of Pharmaceuticals, Tirupati-517502.*

[c]*Department of Pharmaceutical Chemistry, Sri Padmavathi School of Pharmacy, Tirupathi-517503, Andhra Pradesh, India.*

[d]*Senior lecturer in Pharmacy, SVMP Womens Polytechnic College, Tirupati.*

***Corresponding author E-mail address**: krishna.supraja@gmail.com (Supraja N.)

ISSN: 2582-3353

Crossref

Publication details
Received: 10th September 2020
Revised: 12th October 2020
Accepted: 12th October 2020
Published: 07th November 2020

Abstract: Synthesis of metal nanoparticles using biological systems is an expanding research area in nanotechnology. Moreover, search for new nanoscale antimicrobial is been always attractive as they find numerous avenues for application in medicine. Bio synthesis of metallic nanoparticles is cost effective and eco-friendly compared to those of conventional methods of nanoparticles synthesis. Herein, we reported a green and simple method for bio synthesizing silver nanoparticles (AgNPs) using Carica papaya leaf, peel and seed extracts as reducing and stabilizing agent. FTIR, XRD, UV–VIS spectroscopy, and DLS have been used for characterizing the bio synthesized AgNPs. The results indicating the AgNPs synthesized by Carica papaya leaf, peel and seed extracts have high purity and the average size is 90 nm. The antioxidant property was studied by radical scavenging (DPPH) assay, antimicrobial activity of AgNPs was evaluated (in vitro) against fungi, Gram-negative, and Gram-positive bacteria using disk diffusion method. Anti-corrosion studies were carried out using coupon method (mild steel) and photo-catalytic activity of the AgNPs has been investigated by degradation methylene blue under visible light irradiation. Due to the smaller size, the biosynthesized AgNPs showed an excellent photo-catalytic (Dye degradation) performance. The synthesized AgNPs exhibited effective anti-cancerous activity (at doses 1 and 40µg/ml of AgNPs) against Chinese hamster ovary cancer cell lines.

Keywords: Carica papaya leaf; peel; seed extracts; Antimicrobial activity; Antioxidant activity; photo-catalytic activity; Anti-cancerous activity; Corrosion studies

1. Introduction

The development of green processes for the synthesis of nanoparticles has been evolving into an important branch of nanotechnology as green nanotechnology deals with the safe and eco-friendly methods for nanomaterials fabrication and which is considered as an alternative to conventional physical and chemical methods.[1] Nanomaterials exhibit unique and considerably changed physical, chemical, and biological properties compared to their bulk counterparts.[2] Although physical and chemical methods[3] are more popular for nanoparticle synthesis, the use of toxic compounds limits their applications.[4] Indeed, over the past several years, plants, algae, fungi, bacteria, and viruses have been used for production of metallic nanoparticles.[5] Green synthesis of metallic nanoparticles from plants[6] is been an interesting aspect as the process is ecofriendly and non-toxic. Plant and plant materials have become potential sources for the synthesis of metallic nanoparticles recently. A number of researchers have reported on synthesis of metallic nanoparticles including silver,[7] gold,[8] titanium dioxide,[9] tungsten oxide,[10] and copper oxide[11] using different plant materials. But reports on synthesis of zinc nanoparticles using plant materials are scant.[12]

Papaya, a tropical fruit, often seen in orange- red, yellow green and yellow orange hues with a rich orange pulp. Whole plant parts, fruits, roots, bark, peel, seeds and pulp are known to have medicinal properties. It has been used for the treatment of numerous diseases like warts, corns, sinuses, eczema, cutaneous tubercles, blood pressure, dyspepsia, constipation, amenorrhoea, general debility, expel thread worms and stimulate reproductive organs It also effectively treats and improves all types of digestive and abdominal disorders.[13] Leaves of papaya, one of the plant part with numerous medicinal value has the history of steaming and eating with spinach in Asia. It has found to have significant effect on various tumor cell lines and the tea extract of leaves found to have antimalarial and antispasmodic activities. It has found to increase the appetite, ease menstrual pain and relieve nausea. Most important traditional use of leaf juice is its capability to increase white blood cells & platelets, normalizes clotting and also repairs the liver.[14] Ayurvedic literature reveals that papaya leaf extract has haemostatic properties and recent studies on ability of C. papaya leaf aqueous extract on platelet augmentation in

cyclophosphamide induced thrombocytopenia rat model was studied and found significant effects.[15] Pilot studies done in dengue patients with leaf juice revealed the effect of leaf Juice on elevating white blood cells, platelet count and recovery without hospital admission. This demand the need for the photochemical profiling of the leaf juice to identify the bioactive constituents attributing significant activity

An extensive literature survey shows that there are no research reports available for synthesis, characterization of Carica papaya silver nanoparticles by leaf, peel and seed extracts Hence, in the current study, we reports for the first time Carica papaya mediated synthesized silver nanoparticles and its applications were conducted for industrial and medical purposes.

2. Materials and Methods

Chemicals Silver nitrate (≥99 % pure) was purchased from Sigma Aldrich, India. Potato dextrose broth, Potato dextrose agar, DPPH, Nutrient broth, and Nutrient agar plate were supplied by Hi-media, India.

2.1. Collection of plant material

Healthy Carica papaya leaf, peel and seed were collected from Acharya N G Ranga Agricultural University, Regional Agricultural Research Station, Tirupati, Andhra Pradesh state, India. From the selected plant, leaf, peel and seed was collected by scrapping using neat and clean knife during the month of October 2018, and collected material was carefully washed and dried at 45°C to constant weight. The dried bark of plant material was powdered, passed through a BSS no. 85-mesh sieve, and stored in air-tight container.

2.2. Preparation of aqueous bark extract

The collected Carica papaya leaf, peel and seed was allowed to shade dried for 72h and was ground to get fine powder. Then, 10 g of powder was mixed with 100mL of distilled water and boiled for 30 min. After that, the extract was filtered by using Whatman No. 1 filter paper and collected the filtrate in plastic bottle and stored at 4°C for further experimentation.

2.3. Collection of microbes

The microbes were collected from NCIM (National Collection of Industrial Microorganisms), Pune, Maharashtra. The bacterial names are E.Coli-NCIM 2068, Pseudomonas- NCIM 5070, Bacillus pantothenticus- NCIM 2476, Staphylococcus aureus- NCIM 2127 and Salmonella typhimurium- NCIM 2501. The fungal names are Aspergillus flavus- NCIM 1316, Aspergillus Niger- NCIM 1025, Fusarium oxysporium- NCIM 1043 and Rhizopus stolonifer- NCIM 1139.

2.4. Preparation of Carica papaya (Leaf, Peel and Seed) Ag nanoparticles

10 ml of 10 % aqueous extract of Carica papaya (Leaf, Peel and Seed) was added in to 90 ml of aqueous solution of 1 mM Silver nitrate. The mixture was exposed to a range of controlled temperatures for 24 h. Appearance of brown color in solution indicated the formation of AgNPs. The solution was then kept in dark for further analysis collected and stored at 4°C for further use. The samples were then centrifuged using REMI K70 at 4000 rpm (2146 g) for 15 min to get clear supernatant. The initial concentration of the extracts was measured using inductively coupled plasma optical emission spectrophotometer (ICP-OES) then, the sample was diluted to different concentrations of 170, 100, and 50 ppm and they were used to investigate the concentration-dependent antimicrobial effect of extracts.

2.5. Concentration of Carica papaya (Leaf, Peel and Seed) silver nanoparticles is measured using inductively coupled plasma optical emission spectrophotometer (ICPOES) (Prodigy XP, Leeman Labs, USA)

The concentrations of the Carica papaya extracts were measured using ICP-OES (Prodigy XP, Leeman Labs, USA). The samples were prepared with ten times dilution after centrifugation at 4000 rpm for 15 min. Then, 20 ml of aliquot was loaded to the racks of automatic sampler, and the concentration of Carica papaya extracts mediated synthesized silver nanoparticles was estimated thrice.

2.6. Characterization of Zn nanoparticles

2.6.1. UV–visible spectrum for synthesized nanoparticles

The bio-reductant nanoparticles were monitored by UV– visible (UV–vis) spectrum at various time intervals. The UV–vis spectra of this solution were recorded (UV- 2450, SHIMADZU Spectrophotometer) from 200 to 400 nm.

2.6.2. FT-IR analysis for synthesized nanoparticles

The FTIR spectrum was taken in the mid-IR region of 400–4000 cm^{-1}. The spectrum was recorded using ATR (attenuated total reflectance) technique. The dried sample was mixed with the KBr (1:200) crystal, and the spectrum was recorded in the transmittance mode (Tensor 27, BRUKER).

2.6.3. X-ray diffraction (XRD) analysis for synthesized nanoparticles

The phyto-reduced nanoparticles were characterized to reveal their crystal structure using X-ray diffraction technique. The XRD pattern was recorded using computer controlled XRD-system (JEOL, and Model: JPX-8030) with CuKa radiation (Ni filtered = 13418 A°) in the range of 40 kV, 20 A. The built-in software (syn master 7935) program was used for the identification of XRD peaks corresponding to the Bragg's reflections.

2.6.4. Particle size and zeta potential analysis of Ag nanoparticles

The aqueous suspension of the synthesized nanoparticles was filtered through a 0.22-lm syringe driven filter unit, and the size and distribution of the nanoparticles were measured using dynamic light scattering technique (Nanopartica, HORIBA, SZ-100).

Fig. 1. Photograph showing *Carica papaya* (a) leaf (b) peel and (c) seed extracts

2.7. Assay for antimicrobial activity of Carica papaya extracts (Leaf, Peel and Seed)

The antimicrobial activity of Carica papaya extracts was determined on the basis of colony formation (CFU) by in vitro Petri dish assays (disk diffusion). Each fungal and bacterial isolates were cultured on growth media that induced prolific conidia and bacterial production. The fungi isolates were grown on potato dextrose agar medium, and bacterial isolates were grown on nutrient agar medium. Conidia were collected from cultures that were incubated at 37°C for 10 days (fungi), and bacterial cultures were collected from cultures that were incubated at 37°C for 2 days for (bacteria) and diluted with sterile, deionized water to a concentration of 106 spores ml^{-1}. Aliquots of the conidial suspension and bacterial suspensions were mixed with serial concentrations of silver preparations to a final volume of 1 ml and were also mixed with sterile, deionized water as control. A 10µl subsample of the conidia and Carica papaya extracts Ag mixture stock was taken at 50 ± 0.9, 100 ± 1.1 and 170 ± 1.4 ppm after Ag treatments and diluted 100-fold with the deionized water. A 10 µl aliquot of the diluted spore suspension was spread on PDA (Becton, Dickson and Company, Sparks, MD) medium. Three PDA plates for fungi and three NA plates for a bacterium per each combination of exposure Carica papaya extracts of silver nanoparticles concentration were tested. The filter paper disk was dipped in different ppm and inserted on mediums (PDA and NA), and then the plates were incubated at 37°C for 2–4 days for fungi and bacteria, respectively. The average number of colonies from silver-treated spore suspensions (fungi) and (bacteria) was compared with the number on the water control (percent colony formation). The zone size was determined by measuring the diameter of the zone in mm.[16]

2.8. Dye degradation (Methylene blue) studies by using Carica papaya extract (Leaf, Peel and Seed)

Typically 5drops of methylene blue dye was added to 1000 mL of double distilled water used as stock solution. About 8 mg of biosynthesized silver nanoparticles Carica papaya extract (Leaf, Peel and Seed) was added to 100 mL of methylene blue dye solution. A control was also maintained without addition of silver nanoparticles. Before exposing to irradiation, the reaction suspension was well mixed by being magnetically stirred for 40min to clearly make the equilibrium of the working solution. Afterwards, the dispersion was kept under the sunlight and monitored from morning to evening sunset. At specific time intervals, aliquots of 2-3 mL suspension were filtered and used to evaluate the photo-catalytic degradation of dye.

The absorbance spectrum of the supernatant was subsequently measured using UV-Vis spectrophotometer at the different wavelength. The initial concentration of dye was measured by UV–Vis spectroscopy the absorbance value shown at 290 nm.[17]

2.9. Anticancer activity of Carica papaya extracts (Leaf, Peel and Seed) using Chinese hamster ovary (CHO) cell line and treatment procedure

CHO cells were obtained from National Centre for Cell Sciences (NCCS), Pune, India. The CHO cells were grown at 37 ^{o}C in humidified incubator under 5% CO_2 / 95% air in DMEM with 10% fetal bovine serum (FBS). CHO cells were seeded in 96- well plates at the quantity of 0.2x106 cells per well. CHO cells were treated with test compounds for 24 h in a humidified CO_2 incubator. At the end 20µL of 5mg/mL MTT (3-(4,5-dimethylthiozol-2-yl)-2,5-diphenyltetrazoliumbromide) was added and incubated for 4 h in humidified atmosphere followed by the addition of 200µL of DMSO to the wells to dissolve the MTT formazan crystals. In a control experiment, cells were grown in a same media without test compounds. Absorbance was recorded at 570 nm immediately after the development of purple color. The formazan generated in the control cells was considered to represent 100% viability. Relative cell viability was evaluated according to the quantity of MTT converted into insoluble formazan salt. Three independent experiments were carried out and mean ± S.E.M was calculated and reported as (%) of cell viability vs concentration (µM).[18] (Dhandapani Kayal Vizhi et al. 2016.

2.10. Antioxidant studies for Carica papaya extracts (Leaf, Peel and Seed) mediated synthesized AgNPs

2.10.1. Quantitative analysis

Each compound was dissolved in methanol 10 mg/10 mL and it was used as stock solution. From the stock solutions 1 mL of each compound solution with different concentrations

(0.25–1.00 lg) were added to the 3 mL of methanolic DPPH (0.004%) solution. After 30 min, the absorbance of the test compounds was taken at 517 nm using UV–VIS spectrophotometer, which was compared with the corresponding absorbance of standard BHT concentrations (0.25–1.00 lg). DPPH solution was used as control without the test compounds, whereas methanol was used as blank.[19] The percentage of scavenging activity of DPPH free radical was measured by using the following formula

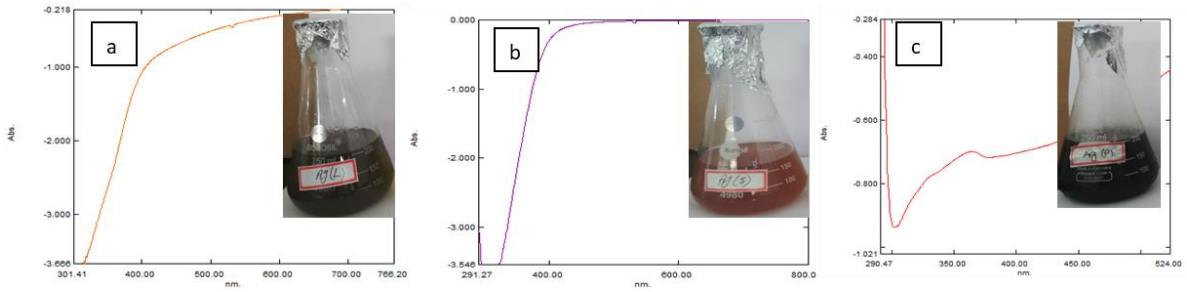

Fig. 2. UV–visible spectroscopic micrograph showing the localized surface Plasmon resonance (LSPR) of Ag nanoparticles synthesized using *Carica papaya* (a) leaf (b) peel and (c) seed extracts

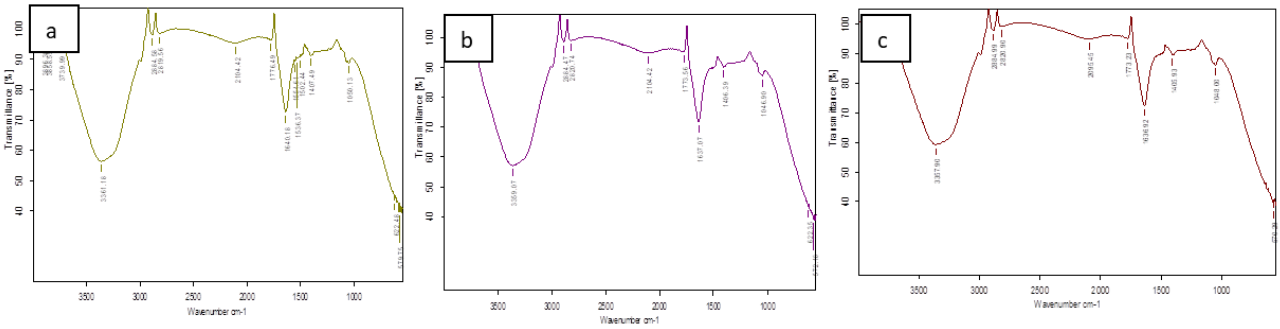

Fig. 3. FT-IR spectroscopic micrograph representing the functional groups responsible for the reduction and stabilization of Ag nanoparticles synthesized using *Carica papaya* (a) leaf (b) peel and (c) seed extracts.

Scavenging activity (%) = A_0-A_i/A_0 ×100

Where A_0 is the absorbance of the control and A_i is the absorbance of the sample. IC50 values were calculated for compounds, which exhibited the significant activity. IC50 is defined as concentration sufficient to obtain 50% of maximum scavenging activity.[20]

2.10.2. Statistical analysis

All of the data from three independent replicate trials were subjected to analysis using Statistical package for the Social Sciences (SPSS) version 16.0. The data are reported as the mean ± SD.

3. Results and Discussions

3.1. UV-visible spectrum analysis

Once the Carica papaya leaf, peel and seed extracts (Fig. 1) UV–visible spectroscopy is an important technique to determine the formation and stability of metal Nanoparticle in aqueous solution. The color changes arise because of the excitation of surface Plasmon resonance arising due to the group of free conduction electrons induced by an interacting electromagnetic field in the silver Nanoparticle. It shows yellowish to dark brown in colour (Fig. 2a, b and c). The strong surface Plasmon resonance band appears at the range of 410 nm in Carica papaya leaf, 400 nm in Carica papaya peel, 370 nm in Carica papaya seed and the broadening of peak indicated that the particles are monodispersed.[18]

3.2. FT-IR analysis

FT-IR measurement was carried out to identify the possible bio-molecules responsible for capping and efficient stabilization of Ag Nanoparticle synthesized using Carica papaya extracts (Leaf, Peel and Seed). The spectrum of Carica papaya leaf shows lot of absorption bands (Fig. 3a) indicates the presence of active functional groups in the synthesized silver Nanoparticles. The intensity peaks are slightly increased for the period of silver nanoparticle synthesis like 3896, 3858, 3739, 3361, 2884, 2819, 2104, 1776, 1640, 1661, 1536, 1502, 1407, 1050, 622 and 579 cm^{-1}. The band present at 3896, 3858, 3739, 3361 corresponds to N-H, O-H Stretching vibrations of alkanes, 2884, 2819 amide, alcohol and H–bonded to phenols. The peak at 2104, 1776, 1640, 1661 indicate to C=C, C=O stretching vibrations to alkenes and amide. The peak at 1536, 1502, 1407 represents to C-Hin plane bend to alkenes. The peak at 579 corresponds to C-Cl, C-Br stretching vibrations to alkyl halides. The band at 1050, 622 corresponds to C-N stretching vibration.

FT-IR spectrum of the biosynthesized silver nanoparticles using Carica papaya peel extract (Fig.3b) shows the absorption peaks at 3359, 2884, 2820, 2104, 1773, 1637, 1406, 1046, 622 and 572 cm^{-1}. The peak present at 3359cm^{-1} reveals the presence of C-H stretching vibration of alkynes, 2884 and 2820 cm^{-1} reveals the presence of C-H stretching vibration of alkanes, 2104 cm^{-1} reveals the presence of C-H stretching vibration of aldehydes, 1773 cm^{-1} reveals the presence of -C=C- stretching vibration of alkynes, 1637 cm^{-1} reveals the presence of –C=C- stretching vibration of alkenes, 1406 cm^{-1} reveals the presence of C-C stretching vibration of aromatics, 1046 cm^{-1} reveals the presence of C-N stretching vibration of aliphatic amines, 622 and 572 cm^{-1} reveals the presence of C-Br stretching vibration of alkyl halides.

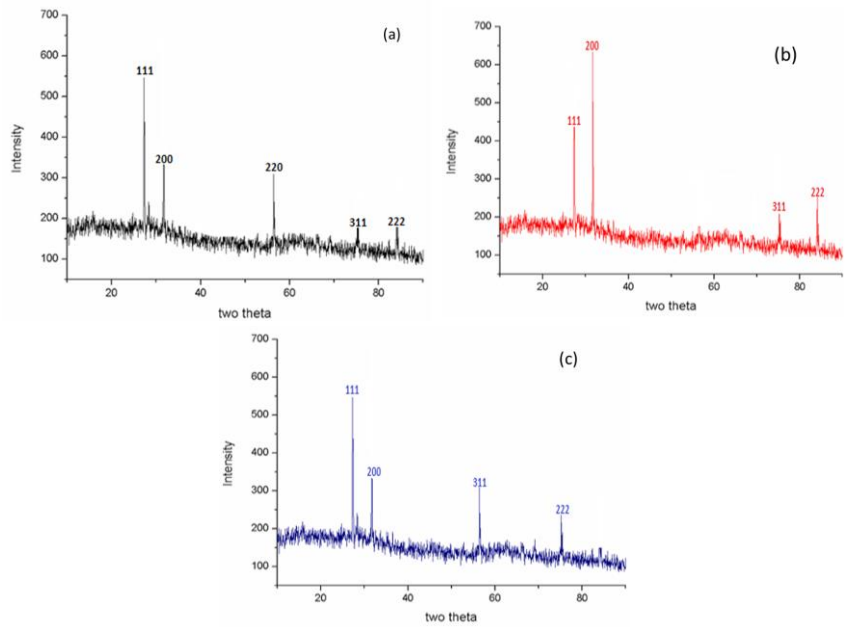

Fig. 4. XRD micrograph with the recorded Bragg's reflections corresponds to the FCC crystal structure of the silver nanoparticles synthesized using *Carica papaya* seed extract

FT-IR spectrum of the biosynthesized silver nanoparticles using Carica papaya seed extract (Fig. 3c) shows the absorption peaks at 3357, 2884, 2820, 2095, 1773, 1636, 1408, 1048 and 570 cm^{-1}. The peak present at 3357 cm^{-1} reveals the presence of C-H stretching vibration of alkynes, 2884 cm^{-1} reveals the presence of C-H stretching vibration of alkanes, 2820 cm^{-1} reveals the presence of -C=C- stretching vibration of alkynes. 2095 and 1773 cm^{-1} reveals the presence of C=O stretching vibration of carboxylic acids, 1636 cm^{-1} reveals the presence of N-H bend stretching vibration of primary amines, 1408 cm^{-1} reveals the presence of C-H bend stretching vibration of alkanes, 1048 cm^{-1} reveals the presence of C-H wag stretching vibration of alkyl halides and 570 cm^{-1} reveals the presence of C-Br stretching vibration of alkyl halides. Primary amine groups of N–H bending and carbonyl stretching vibrations of protein, respectively, indicating the involvement of proteins in reduction and stabilization of silver ions. The nanoparticles are bound to the functional organic groups (carboxyl and amine) from the Carica papaya extracts, and these functional groups may act as template, reducing and capping agents of silver nanoparticles.

FT-IR studies confirm that the carbonyl groups from the amino acid residues and proteins have the stronger ability to bind AgNPs to prevent agglomeration and thereby stabilize the AgNPs through free amine groups in proteins.[21]

3.3. X-Ray diffraction analysis

X-ray diffraction pattern of Carica papaya extracts (Leaf, peel and seed) mediated synthesis of silver nanoparticles shows the peaks correspond to the Bragg's reflections of (111), (200), (220), (311) and (222) planes, which confirms the face-centered cubic (FCC) crystalline structure of silver (Fig. 4a, b and c). XRD analysis showed intense peaks at 2θ values of 27.08°, 36.43º, 58.82°, 78.87° and 86.87° corresponding to Bragg's reflection based on the fcc structure of silver nanoparticles. The intensity data were collected over a 2θ range of 10°–90°. A definite line broadening of the XRD peaks indicates that the prepared material consists of particles in nanoscale range. This clearly indicates that the silver nanoparticles formed by the reduction of Ag+ ions by the Carica papaya extracts are crystalline in nature. The relatively higher intensity of (111), (200),

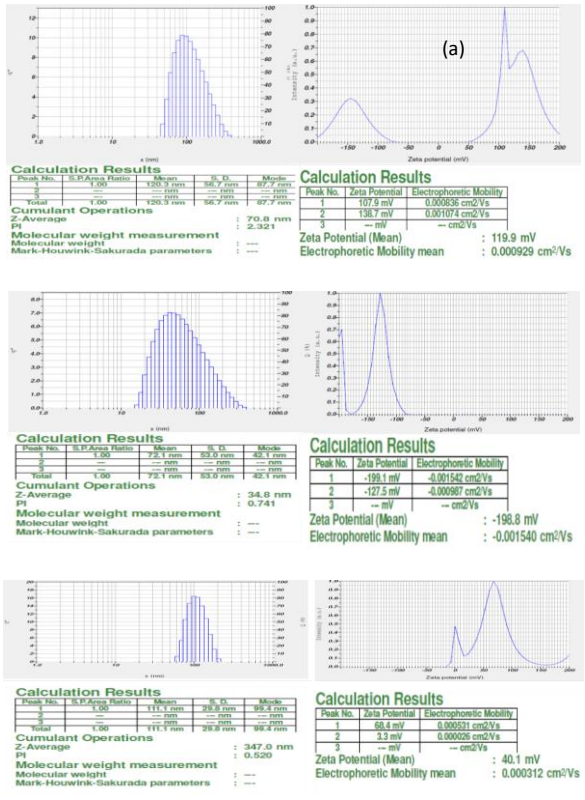

Fig. 5. Histogram (size distribution) of silver nanoparticles (dynamic light scattering) and zeta potential **(a)** (119.9 mV) **(b)** (-198.8 mV) **(c)** (40.1 mV) of silver nanoparticles synthesized using *Carica papaya* leaf extract.

(220), (311) and (222).[8] A representative XRD profile of the silver nanoparticle displaying the structural information and crystalline nature of the silver Nanoparticle synthesized from aqueous extracellular Carica papaya extract (Fig. 4a, b and c).

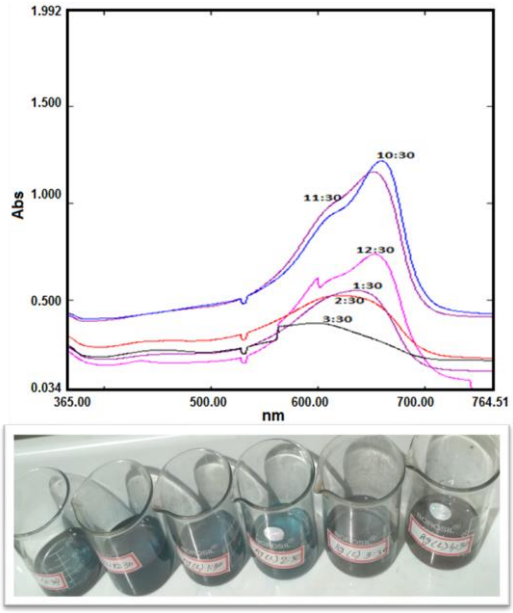

Fig. 6. Photo-catalytic degradation of methylene blue using *Carica papaya* leaf extract mediated silver nanoparticles at different time

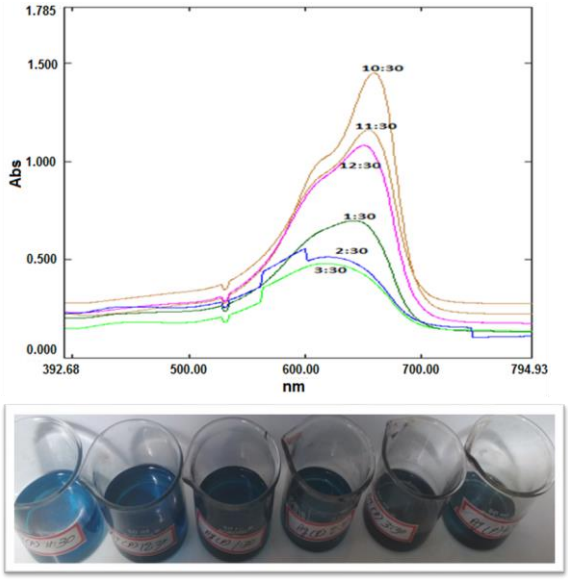

Fig. 7. Photo-catalytic degradation of methylene blue using *Carica papaya* peel extract mediated silver nanoparticles at different time intervals

Table 1. *In-vitro* antioxidant studies using Extracts (Leaf, Peel and seed) mediated silver nanoparticles

Concentration (mg/ml)	% Scavenging activity		
	Ag Leaf	Ag Peel	Ag Seed
0.25	0.010	0.116	0.121
0.50	0.114	0.153	0.145
0.75	0.159	0.172	0.197
1.0	0.198	0.182	0.206
IC_{50} (mg/ml)	0.37	0.31	0.41

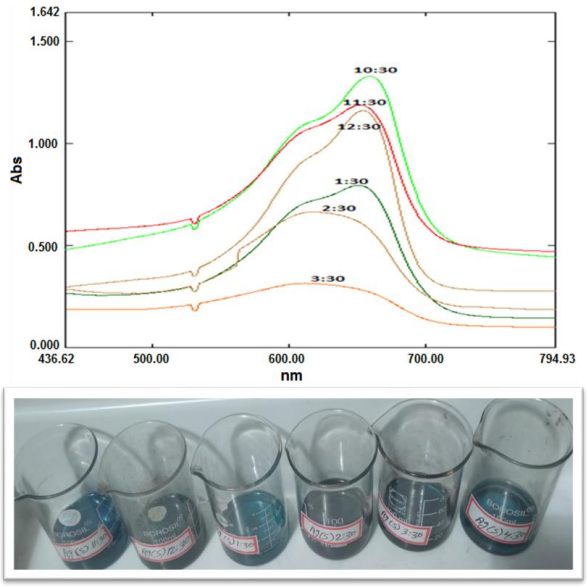

Fig. 8. Photo-catalytic degradation of methylene blue using *Carica papaya* seed extract mediated silver nanoparticles at different time intervals.

3.4. Dynamic light scattering analysis

Particle size and zeta potential values were measured using Nanopartica SZ-100. The particle size distribution spectra for the silver nanoparticles were recorded as diameter (nm) verses frequency (%/nm) spectra with diameter (nm) on x-axis and frequency (%/nm) on y-axis. The zeta potential spectra for the silver nanoparticles were recorded zeta potential verses intensity spectra with zeta potential (mV) on x-axis and intensity (a.u) on y-axis. Particle size of 70.8 nm with zeta potential of 119.9 mV was recorded for the Carica papaya leaf (Fig. 5a), 42.1 nm with zeta potential of -198.8 mV was recorded for the Carica papaya peel (Fig. 5b), 99.4 nm with zeta potential of 40.1mV was recorded for the Carica papaya seed silver nanoparticles synthesized from Carica papaya extracts (Fig. 5c). The zeta potential indicates the degree of repulsion between adjacent and similarly charged particles in dispersion, least particle size and high zeta potential values were recorded.[3] The zeta potential value indicated good stability with high potential. Particle size is measured by the SZ-100 using dynamic light scattering (DLS). The direction of the particle motion determines if the charge is negative or positive, and the speed of the particles determines the magnitude of the charge (zeta potential). The reported zeta potential result can then be used as an indicator of the dispersion stability.

3.5. Photo-catalytic activity of dye degradation studies

Photo-catalytic degradation of methylene blue was carried out by using green synthesized silver nanoparticles under solar light. Dye degradation was initially identified by color change. Initially, the color of dye shows deep blue color changed into light blue after the 1 h of incubation with silver nanoparticles while exposed to solar light (Fig. 6, 7 and 8). There after light blue was changed into light blue. Finally, the degradation process was completed at 24 h and was identified by the change of reaction mixture color to colorless. Photo-catalytic activity of silver nanoparticles on degradation of dye was demonstrated by using the dye methylene blue. The degradation of

Table 2. Anticancer activity of *Carica papaya* extracts (Leaf, Peel and Seed) mediated synthesized silver nanoparticles

	Ag(L)	Ag(P)	Ag(S)
Control	100	100	100
1 µg	91.43831	94.22525	108.7518
2 µg	83.46485	95.58824	78.51506
3 µg	73.2066	69.36872	68.7231
4 µg	69.04591	76.36298	60.07891
5 µg	55.73888	70.5165	47.16643
10 µg	55.55954	53.29986	36.22669
20 µg	36.5495	35.72453	37.62554
30 µg	24.74892	23.88809	32.85509
40 µg	18.11334	15.81779	21.05452
IC_{50}	3.43988 +/- 169.1 (4915%)	3.43433 +/- 231.3 (6734%)	3.34883 +/- 6961 (2.079e+05%)

methylene blue was carried out in the presence of silver nanoparticles at different time in the visible region. The absorption spectrum showed the decreased peaks for methylene blue at different time intervals (10:30-03:30). Initially, the absorption peaks at 650 nm for methylene blue dye were decreased gradually with the increase of the exposure time and that indicates the photo-catalytic degradation reaction of methylene blue.[17] The absorption peak of methylene blue dye was decreased, and absorption band for silver nanoparticles was increased at 480 nm. The completion of the photo-catalytic degradation of the dyes is known from the gradual decrease of the absorbance value of dye approaching the base line and increased peak for silver nanoparticles. While decreasing the concentration of dye, UV spectra show typical SPR band for silver nanoparticles at 7 h of exposure time. The degradation of dye was increased as increasing the exposure time of dye silver nanoparticles complex in sunlight. Absorption peak for methylene blue dye was cantered at 660 nm in visible region which diminished and finally it disappeared while increasing the reaction time, which indicates that the dye had been degraded. But when compared to Carica papaya leaf and peel the Carica papaya seed mediated synthesized silver nanoparticles shown best results in photo-catalytic activity of dye degradation.

3.6. Antioxidant activity of Carica papaya extracts (Leaf, Peel and Seed) mediated AgNPs

For obtained protein capped silver nanoparticles, we evaluated in vitro antioxidant activity against to 2,2-diphenyl- 1-picrylhydrazyl (DPPH) free radical. The hydrogen atom or electron donation ability of the silver nanoparticles and the pure Carica papaya extracts were measured from the bleaching of a purple-coloured ethanol solution of DPPH. Because DPPH and peroxyl radicals have similar electronic structures (the unpaired electron is delocalized over both N atoms of hydrazyl and both O atoms of peroxyl), the reaction rate of DPPH and antioxidants gives a good approximation for scavenging activities with lipid peroxyl radicals. This spectrophotometric assay uses the stable radical 2,2-diphenyl-1-picrylhydrazyl (DPPH) as a reagent. Antioxidant property was evaluated using DPPH which showed increase in free radical scavenging activity of the silver nanoparticles, which increased with the increase in concentration of the nanoparticles.

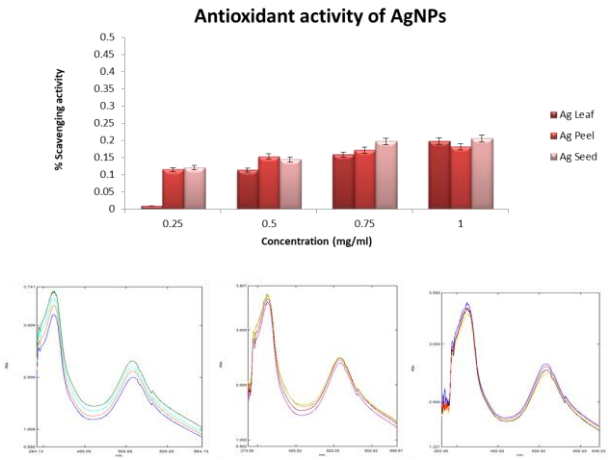

Fig. 9. Antioxidant activity of Carica papaya (a) leaf (b) Peel and (c) seed extract-mediated synthesized AgNPs.

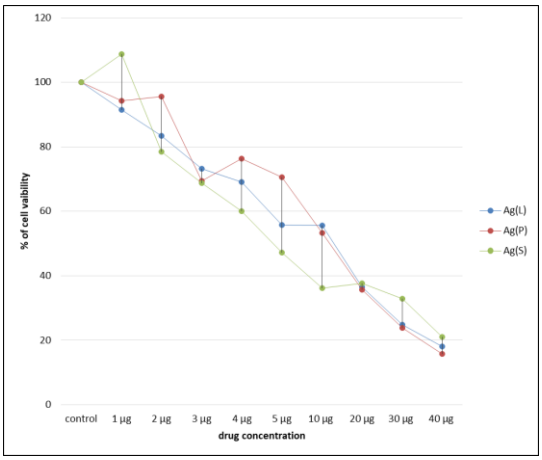

Fig. 10. Anticancer efficacy (Chinese hamster ovary) of *Carica papaya* (a) leaf (b) Peel and (c) seed extract-mediated synthesized AgNPs

DPPH radical scavenging assay was investigated for the evaluation of antioxidant potential of the prepared hydrogel formulations. The purple solution containing DPPH turns yellow on addition of formulation, which indicates the scavenging of free radicals and presence of antioxidant activity. The antioxidant activity of the aqueous extracts of Carica papaya AgNPs was evaluated using DPPH scavenging assays. As shown in (Table. 1), a significant difference was observed among the respective values obtained.[22,23] The DPPH values were increased in a dose dependent manner. The recorded value for the lowest concentration of the aqueous extract (0.25 mg/L) was 0.010 in leaf, 0.116 in peel and 0.121 in seed, in (0.50 mg/mL) 0.114 in leaf, 0.153 in peel and 0.145 in seed, in (0.75 mg/mL) 0.159 in leaf, 0.172 in peel and 0.197 in seed, in (1 mg/mL) 0.198 in leaf, 0.182 in peel and 0.206 in seed and this value was increased when the concentration was increased to 1 mg/L. However, IC50 values recorded for Carica papaya leaf 0.37 mg/mL, IC50 values recorded for Carica papaya peel 0.31 mg/mL and IC50 values recorded for Carica papaya seed 0.41 mg/mL. Interestingly, the results of Carica papaya seed extract shown very good antioxidant activity when compared to Carica leaf and peel in a dose dependent manner (Fig. 9)

Table 3. *In-vitro* antibacterial studies against bacterial pathogens using Extracts (Leaf, Peel and seed) mediated silver nanoparticles

S. No	Bacterial names	*Carica papaya* extracts (Leaf, Peel and Seed) silver nanoparticles Zone of inhibition (mm)								
		Leaf extract			Peel extract			Seed extract		
		170ppm	100ppm	50ppm	170ppm	100ppm	50ppm	170ppm	100ppm	50ppm
1	*E. Coli- NCIM-2068*	1.5±0.05	1.1±0.02	1.0±0.8	2.0±0.2	1.7±0.8	1.0±0.4	4.0±0.9	3.8±0.6	1.9±0.3
2	*Pseudomonas- NCIM-5070*	2.1±0.09	1.6±0.01	1.3±0.7	1.7±0.07	1.2±0.01	1.0±0.6	2.5±0.4	2.0±0.9	1.9±0.4
3	*Bacillus pantothenticus-NCIM-2476*	1.6±0.08	1.2±0.02	1.0±0.6	1.7±0.08	1.2±0.04	1.1±0.6	4.8±0.05	2.0±0.01	1.9±0.7
4	*Staphylococcus aureus-NCIM-2127*	2.2±0.09	1.6±0.05	1.4±0.01	4.5±0.02	2.5±0.5	0.8±0.2	4.0±0.03	3.8±0.8	1.0±0.4
5	*Salmonella typhimurium-NCIM-2501*	4.5±0.06	4.0±0.03	2.5±0.9	3.0±0.05	1.5±0.01	1.4±0.6	2.6±0.03	1.6±0.4	1.0±0.2

Table 4. *In-vitro* antifungal studies against fungal pathogens using Extracts (Leaf, Peel and seed) mediated silver nanoparticles

S. No	Fungal names	*Carica papaya* extracts (Leaf, Peel and Seed) silver nanoparticles Zone of inhibition (mm)								
		Leaf extract			Peel extract			Seed extract		
		170ppm	100ppm	50ppm	170ppm	100ppm	50ppm	170ppm	100ppm	50ppm
1	*Aspergillus flavus-NCIM 1316*	2.8±0.07	2.2±0.02	1.9±0.5	4.0±0.05	3.5±0.01	3.3±0.6	3.5±0.07	2.4±0.02	2.2±0.8
2	*Aspergillus Niger- NCIM-1025*	4.2±0.09	3.6±0.03	1.5±0.7	4.3±0.07	4.0±0.04	3.8±0.02	3.5±0.06	3.0±0.02	2.6±0.8
3	*Fusarium oxysporium- NCIM-1043*	3.5±0.08	2.9±0.02	2.6±0.4	4.5±0.06	4.3±0.7	4.0±0.3	4.0±0.05	3.9±0.02	3.6±0.7
4	*Rhizopus stolonifer- NCIM -1139*	4.0±0.05	3.9±0.9	2.8±0.4	5.0±0.08	4.7±0.03	4.6±0.8	4.5±0.03	4.3±0.8	4.0±0.6

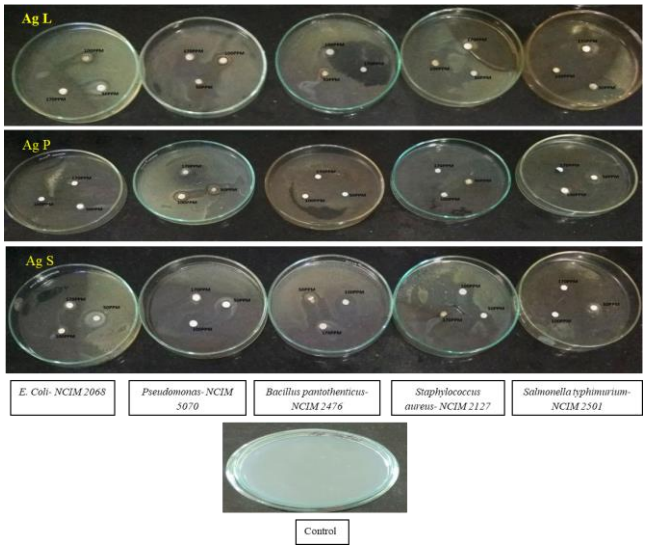

Fig. 11. Antibacterial activity of different concentrations (170, 100 and 50ppm) of *Carica papaya* (a) leaf (b) Peel and (c) seed extract-mediated synthesized AgNPs (**Plate 1.**).

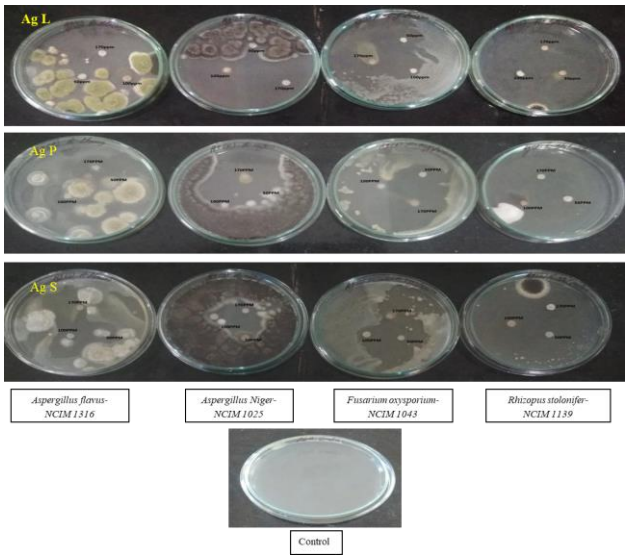

Fig. 12. Antifungal activity of different concentrations (170, 100 and 50ppm) of Carica papaya (a) leaf (b) Peel and (c) seed extract-mediated synthesized AgNPs (**Plate 2)**.

3.6. Anticancer efficacy (CHO) of Carica papaya extracts (Leaf, Peel and Seed) mediated AgNPs

The in-vitro cytotoxicity of the AgNPs was evaluated CHO cell lines at different concentrations (1, 2, 3, 4, 5, 10, 20, 30 and 40). Our cytotoxicity analysis of the sample shows a direct dose-response relationship cytotoxicity increased at higher concentrations. The IC50 value was plotted by taking the concentration of AgNPs on X-axis versus percentage of cell viability on Y- axis (Fig. 10). The samples demonstrated a considerable cytotoxicity against the CHO cell lines. The result showed that CHO cells proliferation were significantly inhibited by AgNPs with an IC50 value of 3.43988+/-169.1 (4915%) µg/ml of the concentration in Carica papaya leaf. IC50 value of 3.43433 +/- 231.3 (6734%) µg/ml of the concentration in Carica papaya peel and IC50 value of 3.34883 +/- 6961 (2.079e+05%) µg/ml of the concentration in Carica papaya seed. As shown in Table.2, in the lowest tested concentration (1µg/ml), AgNPs were able to inhibit the cell line's growth by less than 10%. In contrast the presence of 40µg/ml of AgNPs significantly inhibited the cell line's growth (>95%). But when compared to leaf and peel the seed shown high cytotoxicity effect. Previous study shows that phyto-chemicals deplete intracellular antioxidants thereby induced cancer cell death.[24,25]

3.7. Antimicrobial efficacy of Carica papaya extracts (Leaf, Peel and Seed) mediated AgNPs

AgNPs obtained from Carica papaya extracts (leaf, peel and seed) have shown very strong inhibitory action against fungal sp, Gram-positive and Gram-negative bacteria (Figs. 11 & 12). Three concentrations of AgNPs (170, 100, 50 ppm) were prepared and were applied against an array of fungal species viz, Aspergillus flavus-NCIM 1316, Aspergillus Niger- NCIM-1025, Fusarium oxysporium- NCIM-

Table 5. Weight loss and corrosion study (Bacteria) for mild steel coupons in presence of *Carica papaya* extracts (Leaf, Peel and Seed) mediated synthesized silver nanoparticles

	Weight loss (mg)			Corrosion rate (mm/y)		
System	**Mild steel Ag Leaf**	**Mild steel Ag Peel**	**Mild steel Ag Seed**	**Mild steel Ag Leaf**	**Mild steel Ag Peel**	**Mild steel Ag Seed**
Experiment	Bacteria (*Bacillus pantothenticus*-NCIM-2476)+NPs **0.728**	Bacteria (*Bacillus pantothenticus*-NCIM-2476)+NPs **0.674**	Bacteria (*Bacillus pantothenticus*-NCIM-2476)+NPs **1.378**	Bacteria (*Bacillus pantothenticus*-NCIM-2476)+NPs **0.242**	Bacteria (*Bacillus pantothenticus*-NCIM-2476)+NPs **0.352**	Bacteria (*Bacillus pantothenticus*-NCIM-2476)+NPs **0.568**
	Bacteria (*E.Coli*-NCIM-2068)+NPs **0.365**	Bacteria (*E.Coli*-NCIM-2068)+NPs **0.876**	Bacteria (*E.Coli*-NCIM-2068)+NPs **1.876**	Bacteria (*E.Coli*-NCIM-2068)+NPs **0.121**	Bacteria (*E.Coli*-NCIM-2068)+NPs **0.765**	Bacteria (*E.Coli*-NCIM-2068)+NPs **0.976**
	Bacteria (*Pseudomonas*-NCIM-5070)+NPs **1.197**	Bacteria (*Pseudomonas*-NCIM-5070)+NPs **1.564**	Bacteria (*Pseudomonas*-NCIM-5070)+NPs **1.354**	Bacteria (*Pseudomonas*-NCIM-5070)+NPs **0.399**	Bacteria (*Pseudomonas*-NCIM-5070)+NPs **0.564**	Bacteria (*Pseudomonas*-NCIM-5070)+NPs **0.754**
	Bacteria (*Staphylococcus aureus*-NCIM-2127)+NPs **0.299**	Bacteria (*Staphylococcus aureus*- NCIM-2127)+NPs **1.345**	Bacteria (*Staphylococcus aureus*- NCIM-2127)+NPs **1.765**	Bacteria (*Staphylococcus aureus*- NCIM-2127)+NPs **0.096**	Bacteria (*Staphylococcus aureus*- NCIM-2127)+NPs **0.987**	Bacteria (*Staphylococcus aureus*- NCIM-2127)+NPs **0.765**
	Bacteria (*Salmonella typhimurium*-NCIM-2501)+NPs **0.717**	Bacteria (*Salmonella typhimurium*-NCIM-2501)+NPs **0.980**	Bacteria (*Salmonella typhimurium*-NCIM-2501)+NPs **1.745**	Bacteria (*Salmonella typhimurium*-NCIM-2501)+NPs **0.239**	Bacteria (*Salmonella typhimurium*-NCIM-2501)+NPs **0.834**	Bacteria (*Salmonella typhimurium*-NCIM-2501)+NPs **0.345**
Control	AgNPs 0.046	AgNPs 0.068	AgNPs 0.089	AgNPs 0.076	AgNPs 0.012	AgNPs 0.076

Table 6. Weight loss and corrosion study (Fungi) for mild steel coupons in presence of *Carica papaya* extracts (Leaf, Peel and Seed) mediated synthesized silver nanoparticles

	Weight loss (mg)			Corrosion rate (mm/y)		
System	**Mild steel Ag Leaf**	**Mild steel Ag Peel**	**Mild steel Ag Seed**	**Mild steel Ag Leaf**	**Mild steel Ag Peel**	**Mild steel Ag Seed**
Experiment	Fungi (*Aspergillus niger*-NCIM-1025)+NPs **0.828**	Fungi (*Aspergillus niger*-NCIM-1025)+NPs **0.784**	Fungi (*Aspergillus niger*-NCIM-1025)+NPs **1.398**	Fungi (*Aspergillus niger*-NCIM-1025)+NPs **0.362**	Fungi (*Aspergillus niger*-NCIM-1025)+NPs **0.252**	Fungi (*Aspergillus niger*-NCIM-1025)+NPs **0.656**
	Fungi (*Aspergillus Flavus*-NCIM-1316)+NPs **1.665**	Fungi (*Aspergillus Flavus*- NCIM-1316)+NPs **1.576**	Fungi (*Aspergillus Flavus*-NCIM-1316)+NPs **1.844**	Fungi (*Aspergillus Flavus*-NCIM-1316)+NPs **0.223**	Fungi (*Aspergillus Flavus*- NCIM-1316)+NPs **0.875**	Fungi (*Aspergillus Flavus*-NCIM-1316)+NPs **0.996**
	Fungi (*Fusarium oxysporium*-NCIM-1043)+NPs **1.987**	Fungi (*Fusarium oxysporium*-NCIM-1043)+NPs **1.984**	Fungi (*Fusarium oxysporium*-NCIM-1043)+NPs **1.657**	Fungi (*Fusarium oxysporium*-NCIM-1043)+NPs **0.786**	Fungi (*Fusarium oxysporium*-NCIM-1043)+NPs **0.954**	Fungi (*Fusarium oxysporium*-NCIM-1043)+NPs **0.980**
	Fungi (*Rhizopus stolonifer* -NCIM-1139)+NPs **1.569**	Fungi (*Rhizopus stolonifer*- NCIM-1139)+NPs **1.845**	Fungi (*Rhizopus stolonifer*- NCIM-1139)+NPs **1.905**	Fungi (*Rhizopus stolonifer*-NCIM-1139)+NPs 0.166	Fungi (*Rhizopus stolonifer*- NCIM-1139)+NPs **0.797**	Fungi (*Rhizopus stolonifer*- NCIM-1139)+NPs **0.815**
Control	AgNPs 0.126	AgNPs 0.076	AgNPs 0.190	AgNPs 0.075	AgNPs 0.032	AgNPs 0.045

1043 and Rhizopus stolonifer- NCIM -1139 and bacterial species viz., E. Coli- NCIM-2068, Pseudomonas- NCIM-5070, Bacillus pantothenticus- NCIM-2476, Staphylococcus aureus- NCIM-2127 and Salmonella typhimurium- NCIM-2501 . The higher concentration (170 ppm) of seed mediated synthesized AgNPs showed significant antimicrobial effect (Tables 3 and 4) compared with other concentrations (100, 50 ppm) seen in leaf and peel.

Reports on the mechanism of inhibitory action of silver ions on microorganisms show that upon Ag+ treatment, DNA loses its replication ability and expression of ribosomal subunit proteins as well as some other cellular proteins and enzymes essential to ATP production becomes inactivated. It has also been hypothesized that Ag+ primarily affects the function of membrane-bound enzymes, such as those in the respiratory chain. However, the mechanism of bactericidal actions of silver nanoparticles is still not well understood. In a previous report[26] on the bactericidal activity of silver nanoparticles, it was shown that the interaction between silver nanoparticles and constituents of the bacterial membrane caused structural changes in and damage to membranes, finally leading to cell death.

We speculate that the action of silver nanoparticles is broadly similar to that of silver ion. It may be anticipated that a bacterial cell in contact with silver nanoparticles takes in silver ions, which inhibit a respiratory enzyme(s), facilitating the generation of reactive oxygen species and consequently damaging the cell. The uptake of silver can be recognized by irregular pits. Silver (soft acid) has a greater tendency to react with sulfur- or phosphorus-containing soft bases, such as R-S-R, R-SH, RS−, or PR3. Thus, sulfur-containing proteins in the membrane or inside the cells and phosphorus-containing elements like DNA are likely to be the preferential sites for silver nanoparticle binding. An enlarged image of a part of a severely damaged cell membrane treated with truncated triangular silver nanoplates. It has been suggested[26] that disruption of membrane morphology may cause a significant increase in permeability, leading to uncontrolled transport through the plasma membrane and, finally, cell death. But to understand the mechanisms of action of these agents, more detailed chemical structure elucidation of the bioactive components followed by therapeutic investigations and toxicological assessment are required.[18,27]

3.8. Weight loss (Corrosion coupon study)

Weight loss of mild steel coupons in the presence and absence of bacteria and fungi is presented in (Tables.5&6). In the system presence of bacteria and AgNPs Bacillus pantothenticus-NCIM-2476), the weight loss for Carica papaya leaf AgNPs in coupon 0.728 mg and corrosion rate was 0.242 mm/y, E. Coli- NCIM-2068 the weight loss for coupon 0.365 mg and corrosion rate was 0.121 mm/y, Pseudomonas-NCIM-5070 weight loss for coupon 1.197 mg and corrosion rate was 0.399 mm/y, Staphylococcus aureus-NCIM-2127 weight loss for coupon 0.299 mg and corrosion rate was 0.096 mm/y, Salmonella typhimurium-NCIM-2501 weight loss for coupon 0.717 mg and corrosion rate was 0.239 mm/y and for control Absence of bacteria with nanoparticles weight loss for coupon 2.546 mg and corrosion rate was 2.876 mm/y. Same as shown for fungi and bacteria in peel and seed. It indicates that the corrosion rate was lower in the presence of AgNPs, when compared to bacterial AgNPs and fungal AgNPs which is due to the adsorption of bacteria and fungi with the organic complex AgNPs acts as a good inhibitor for anticorrosion. The reduction of oxygen by bacteria and fungi in the electrolyte is also one of the reasons for the low corrosion rate.[28,18]

4. Conclusions

The present study, it is found that the use of natural renewable and eco-friendly reducing agent used for synthesis of silver nanoparticles exhibits excellent photo-catalytic activity against dye molecules and can be used in water purification systems and dye effluent treatment. The reduction of silver ion peak was measured at 370, 410, 440 nm by UV-visible analysis. Bio-molecules that capped on silver nanoparticles were identified as protein content of seed aqueous extract through FT-IR studies. Crystalline nature of the nanoparticles is evident from bright spots in the SAED pattern, clear lattice fringes in the high-resolution peaks in the XRD pattern, DLS shown small size of nanoparticles with high stability of zeta potential, Zeta potential studies will give strong evidence that these silver nanoparticles have high stability. Effective antioxidant studies against to DPPH free radical was opened new vistas in this green chemistry quest which will directly help to manufacture a novel protein capped silver nano antioxidant. Present investigation also suggests that the biosynthesized silver nanoparticles are exerting in vitro antimicrobial and cytotoxicity studies, anticorrosion activity can be used in prevention of corrosion formation by applying coatings. Looking into all these aspects, it is reasonable to infer that the biosynthesis of silver nanoparticles by Carica papaya extracts (Leaf, Peel and Seed) hopefully might reach this aim because they display novel properties. The biological methods of synthesizing nanoparticles have proved to be one of the best methods so far. This is due to its environment friendly nature and slower kinetics which offer better manipulation and control over crystal growth and stabilization has many advantages such as, process scaling up, economic viability and safe way to produce nanoparticles.

Acknowledgements

Authors are thankful to Acharya N.G. Ranga Agricultural University for providing research facility at institute of Frontier Technology, Regional Agricultural Research Station, Tirupati to carry out this part of the research work.

Conflicts of Interest

The authors declare no conflict of interest.

References

1 Mohanpuria P.; Rana N.K.; Yadav S.K. Biosynthesis of Nanoparticles: Technological Concepts and Future Applications. *J. Nanopart. Res.*, 2008, **10**, 507-517. [CrossRef]
2 Singh R.P.; Shukla V.K.; Yadav R.S.; Sharma P.K.; Singh P.K.; Pandey A.C. Biological Approach of Zinc Oxide Nanoparticles Formation and its Characterization. *Adv. Mater. Lett.*, 2011, **2**, 313-317. [CrossRef]
3 Prasad T.N.V.K.V.; Sudhakar P.; Sreenivasulu Y.; Latha P.; Munaswamy V.; Reddy K.R.; Sreeprasad T.S.; Sajanlal P.R.; Pradeep T. Effect of Nanoscale Zinc Oxide Particles on the Germination, Growth and Yield of Peanut. *J. Plant Nutr.*, 2012, **35**, 905-927. [CrossRef]
4 Salam H.A.; Rajiv P.; Kamaraj M.; Jagadeeswaran P.; Gunalan S.; Sivaraj R. Plants: Green Route for Nanoparticle Synthesis. *Int. Res. J. Biol. Sci.*, 2012, **1**, 85-90. [CrossRef]
5 Thakkar K.N.; Mhatre S.S.; Parikh R.Y. Biological Synthesis of Metallic Nanoparticles. *Nanomed. Nanotechnol. Biol. Med.*, 2010, **6**, 257-262. [CrossRef]
6 Girija S.; Balachandran Y.L.; Kandakumar J. Plants as Green Nanofactories: Application of Plant Biotechnology in Nanoparticle Synthesis-A Review. *Plant Cell Biotechnol. Mol. Biol.*, 2009, **10**, 79-86. [Link]
7 Supraja N.; Prasad T.N.V.K.V.; Gandhi A.D.; Anbumani D.; Kavitha P.; Babujanarthanam R. Synthesis, Characterization and Evaluation of Antimicrobial Efficacy and Brine Shrimp Lethality Assay of Alstonia Scholaris Stem Bark Extract Mediated ZnONPs. *Biochem. Biophys. Rep.*, 2018, **14**, 69-77. [CrossRef]
8 Sreekanth T.V.M.; Nagajyothi P.C.; Supraja N.; Prasad T.N.V.K.V. Evaluation of the Antimicrobial Activity and Cytotoxicity of Phytogenic Gold Nanoparticles. *Appl. Nanosci.*, 2015, **5**, 595-602. [CrossRef]
9 Sundrarajan M.; Gowri S. Green Synthesis of Titanium Dioxide Nanoparticles by Nyctanthes Arbor-Tristis Leaves Extract. *Chalcogenide Lett.*, 2011, **8**, 447-451. [Link]

10 Gunalan S.; Sivaraj R.; Rajendran V. Green Synthesized Zno Nanoparticles against Bacterial and Fungal Pathogens. *Prog. Nat. Sci.: Mater. Int.*, 2012, **22**, 693-700. [CrossRef]
11 Padil V.V.T.; Černík M. Green Synthesis of Copper Oxide Nanoparticles using Gum Karaya as a Biotemplate and their Antibacterial Application. *Int. J. Nanomed.*, 2013, **8**, 889-898. [CrossRef]
12 Supraja N.; Prasad T.N.V.K.V.; Krishna T.G.; David E. Synthesis, Characterization, and Evaluation of the Antimicrobial Efficacy of *Boswellia Ovalifoliolata* Stem Bark-Extract-Mediated Zinc Oxide Nanoparticles. *Appl. Nanosci.*, 2016, **6**, 581-590. [CrossRef]
13 Sudhakar N.; Vidhya R.M.T. Potential Medicinal Properties of Carica Papaya Linn.–A Mini Review. *Int. J. Pharm. Pharm. Sci.*, 2014, **6**, 1-4. [Link]
14 Otsuki N.; Dang N.H.; Kumagai E.; Kondo A.; Iwata S.; Morimoto C. Aqueous Extract of Carica Papaya Leaves Exhibits Anti-Tumor Activity and Immunomodulatory Effects. *J. Ethnopharmacol.*, 2010, **127**, 760-767. [CrossRef]
15 Patil S.; Shetty S.; Bhide R.; Narayanan S. Evaluation of Platelet Augmentation Activity of Carica Papaya Leaf Aqueous Extract in Rats. *J. Pharmacong. Phytochem.*, 2013, **1**, 57-60. [Link]
16 Yamaç M.; Bilgili F. Antimicrobial Activities of Fruit Bodies and/or Mycelial Cultures of Some Mushroom Isolates. *Pharm. Biol.*, 2006, **44**, 660-667. [CrossRef]
17 Supraja N.; Avinash B.; Prasad T.N.V.K.V. *Nelumbo Nucifera* Extracts Mediated Synthesis of Silver Nanoparticles for the Potential Applications in Medicine and Environmental Remediation. *Adv. Nano Res.*, 2017, **5**, 373. [CrossRef]
18 Supraja N.; Dhivya J.; Prasad T.N.V.K.V.; David E. Synthesis, Characterization and Dose Dependent Antimicrobial and Anticancerous Efficacy of Phycogenic (Sargassum Muticum) Silver Nanoparticles against Breast Cancer Cells (MCF 7) Cell Line. *Adv. Nano Res.*, 2018, **6**, 183. [CrossRef]
19 Kavitha P.; Saritha M.; Reddy K.L. Synthesis, Structural Characterization, Fluorescence, Antimicrobial, Antioxidant and DNA Cleavage Studies of Cu (II) Complexes of Formyl Chromone Schiff Bases. *Spectrochim. Acta Part A*, 2013, **102**, 159-168. [CrossRef]
20 Mitiku A.A.; Yilma B. Antibacterial and Antioxidant Activity of Silver Nanoparticles Synthesized using Aqueous Extract of Moringa Stenopetala Leaves. *Afr. J. Biotechnol.*, 2017, **16**, 1705-1716. [CrossRef]
21 Sangeetha R.; Niranjan P.; Dhanalakshmi N. Characterization of Silver Nanoparticles Synthesized using the Extract of the Leaves of Tridax Procumbens. *Res. J. Med. Plant*, **10**, 159-166. [CrossRef]
22 Reddy G.R.; Morais A.B.; Gandhi N.N. 2, 2-Diphenyl-1-Picrylhydrazyl Free Radical Scavenging Assay and Bacterial Toxicity of Protein Capped Silver Nanoparticles for Antioxidant and Antibacterial Applications. *Asian J. Chem.*, 2013, **25**, 9249. [CrossRef]
23 Abdel-Aziz M.S.; Shaheen M.S.; El-Nekeety A.A.; Abdel-Wahhab M.A. Antioxidant and Antibacterial Activity of Silver Nanoparticles Biosynthesized using Chenopodium Murale Leaf Extract. *J. Saudi Chem. Soc.*, 2014, **18**, 356-363. [CrossRef]
24 Wypij M.; Czarnecka J.; Świecimska M.; Dahm H.; Rai M.; Golinska P. Synthesis, Characterization and Evaluation of Antimicrobial and Cytotoxic Activities of Biogenic Silver Nanoparticles Synthesized from Streptomyces Xinghaiensis OF1 Strain. *World J. Microbiol. Biotechnol.*, 2018, **34**, 23. [CrossRef]
25 Rathod D.; Golinska P.; Wypij M.; Dahm H.; Rai M. A New Report of Nocardiopsis Valliformis Strain OT1 from Alkaline Lonar Crater of India and its use in Synthesis of Silver Nanoparticles with Special Reference to Evaluation of Antibacterial Activity and Cytotoxicity. *Med. Microbial. Immunol.*, 2016, **205**, 435-447. [CrossRef]
26 Sondi I.; Salopek-Sondi B. Silver Nanoparticles as Antimicrobial Agent: a Case Study on E. coli as a Model for Gram-Negative Bacteria. *J. Colloid Interface Sci.*, 2004, **275**, 177-182. [CrossRef]
27 Wypij M.; Golinska P.; Dahm H.; Rai M. Actinobacterial-Mediated Synthesis of Silver Nanoparticles and their Activity against Pathogenic Bacteria. *IET Nanobiotechnol.*, 2016, **11**, 336-342. [CrossRef]
28 Maruthamuthu S.; Nagendran T.; Anandkumar B.; Karthikeyan M.S. Palaniswamy N.; Narayanan G. Microbiologically Influenced Corrosion on Rails. *Curr. Sci.*, 2011, **100**, 870-880. [CrossRef]